Bioactive Materials 6 (2021) 2221–2230

Contents lists available at ScienceDirect

Bioactive Materials

journal homepage: www.sciencedirect.com/journal/bioactive-materials

Gold nanorods and nanohydroxyapatite hybrid hydrogel for preventing bone tumor recurrence via postoperative photothermal therapy and bone regeneration promotion

Jinfeng Liao [a,b], Kun Shi [b], Yanpeng Jia [b], Yanting Wu [a], Zhiyong Qian [b,*]

[a] State Key Laboratory of Oral Diseases, National Clinical Research Centre for Oral Diseases, West China Hospital of Stomatology, Sichuan University, Chengdu, 610041, P.R. China

[b] State Key Laboratory of Biotherapy, State Key Laboratory and Collaborative Innovation Center of Biotherapy, West China Hospital, Sichuan University, Chengdu, 610041, Sichuan, P.R. China

ARTICLE INFO

Keywords:
Bone tumor
Gold nanorods
Hybrid hydrogel
Photothermal therapy
Bone regeneration

ABSTRACT

Osteosarcoma is a malignant bone tumor, which often occurs in adolescents. However, surgical resection usually fails to completely remove the tumor clinically, which has been the main cause of postoperative recurrence and metastasis, resulting in the high death rate of patients. At the same time, osteosarcoma invades a large area of the bone defect, which cannot be self-repaired and seriously affects the life quality of the patients. Herein, a bifunctional methacrylated gelatin/methacrylated chondroitin sulfate hydrogel hybrid gold nanorods (GNRs) and nanohydroxyapatite (nHA), which possessed excellent photothermal effect, was constructed to eradicate residual tumor after surgery and bone regeneration. *In vitro*, K7M2wt cells (a mouse bone tumor cell line) can be efficiently eradicated by photothermal therapy of the hybrid hydrogel. Meanwhile, the hydrogel mimics the extracellular matrix to promote proliferation and osteogenic differentiation of mesenchymal stem cells. The GNRs/nHA hybrid hydrogel was capable of photothermal treatment of postoperative tumors and bone defect repair in a mice model of tibia osteosarcoma. Therefore, the hybrid hydrogel possesses dual functions of tumor therapy and bone regeneration, which shows great potential in curing bone tumors and provides a new hope for tumor-related bone complex disease.

1. Introduction

Bone tumor, especially osteosarcoma, is a highly malignant spindle cell sarcoma and produces a tumor-like bone matrix [1]. Osteosarcoma, a severe threat to the health of children and teenagers, mainly occurs in adolescents [2]. Once suffering from osteosarcoma, they may face lifelong disability and even death, which bring heavy blows and losses to families and society. Current clinical treatment options include allogeneic bone transplantation, tumor-inactivated bone, and mechanically processed prosthesis [3,4]. Although limb salvage treatment can be achieved in approximately 60%, the shortcomings are limited allogeneic bone sources, tumor recurrence, and poor biological properties of the processed prosthesis. Consequently, long-term survival rates for osteosarcoma patients remain low and reached a plateau for nearly 40 years [5]. Most osteosarcomas can be removed by surgery. However, it is difficult to ensure that the tumor tissue of the patient's bone tissue is completely removed during the surgery. Residual tumor cells still survive around the bone tissue. Thus, postoperative chemotherapy and radiotherapy should be combined to minimize the recurrence and metastasis induced by residual tumors. The occurrence of serious toxic and side effects such as vomiting, hair loss, and a sharp decrease in the number of white blood cells will greatly affect the quality of life of patients. At the same time, osteosarcoma invasion and surgical intervention will cause a large area of bone defects, making it difficult for the body to repair itself, causing severe pain and lifelong disability to patients. Therefore, pushing the development of bone tumor therapy is a big challenge. Consequently, novel and efficient therapeutic strategies are urgently needed to guide the treatment of bone tumors in clinical problems.

For the clinical practice of surgical resection of osteosarcoma,

Peer review under responsibility of KeAi Communications Co., Ltd.

* Corresponding author.
E-mail address: anderson-qian@163.com (Z. Qian).

https://doi.org/10.1016/j.bioactmat.2021.01.006
Received 15 December 2020; Received in revised form 3 January 2021; Accepted 8 January 2021
Available online 22 January 2021

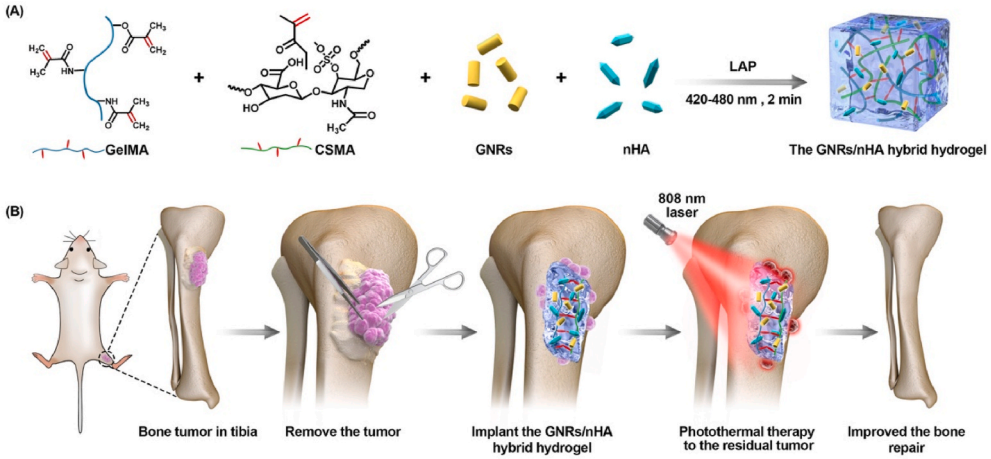

Scheme 1. (A) The schematic preparation of the GNRs/nHA hybrid hydrogel; **(B)** The illustration of the application of the GNRs/nHA hybrid hydrogel for bone tumor photothermal therapy and bone regeneration.

doctors perform extensive resection of the tumor based on the experience of tumor identification and rapid frozen section. However, ensuring that the tumor can be completely resected is still difficult. Coupled with the complex anatomical structure and important nerve blood vessels of the bone, extensive or radical resection faces the problem of reconstructing bone defects after tumor removal. Therefore, eliminating tumors and reducing damage to the normal tissues to the greatest extent is necessary. Tumors that have not been removed during surgery can be completely and effectively eradicated by some auxiliary means. Moreover, photothermal therapy (PTT) is an effective, noninvasive, and non-systemic-toxic tumor treatment method, especially suitable for local treatment of superficial tumors [6–10]. Under the irradiation of near-infrared (NIR) light, photothermal conversion agents (e.g., cyanine dyes, gold nanoparticles, and graphene) can convert the absorbed light energy into heat energy, which can cause tumor cell membrane damage, protein degeneration, and cell decay death or necrosis. Considering the strong NIR absorbance, good biocompatibility, and photothermal stability, gold nanorods (GNRs) have been widely used as an efficient photothermal agent for eradicating tumors [11]. Gold nanoparticle-based PTT showed great potential in preclinical and clinical translation in localized tumor therapy. More recently, gold nanoparticles were applied in prostate tumors by localized PTT in a clinical pilot study [12]. Consequently, short-term local photothermal treatment does not significantly affect the activity of bone marrow mesenchymal stem cells (MSCs) [13,14]. The NIR laser irradiation can reach a limited distance [15,16], and the MSCs located in the bone marrow cavity are relatively safe. Therefore, the photothermal treatment of GNRs is a good strategy for eradicating residual osteosarcoma after surgery.

Osteosarcoma occurs in the epiphyseal end with abundant blood flow. The bone defect caused by the osteosarcoma is large, and the body is having difficulty repairing or healing itself. Therefore, external scaffolds, stem cells, growth factors, or small-molecule drugs are needed [17–20]. Material mechanics, computer-aided digital technology, and bone tissue engineering scaffolds (e.g. hydrogels, microspheres, and 3D printed scaffolds) have been greatly improved in recent years with the continuous development of biomaterials science [21–24]. The hydrogel is a three-dimensional porous mesh gel with abundant water absorbance, good biocompatibility, and degradable structure [25,26]. It can mimic the extracellular matrix (ECM) for the proliferation and differentiation of MSCs to improve bone repair [27]. Thus, it has been widely studied in bone regeneration, due to its excellent biocompatibility, bioactivity, biodegradability, and osteoinductivity [28,29]. Inspired by the dentistry of prosthodontics, blue light-induced photopolymerization is a mild way to initiate monomer polymerization [30–32]. In the hydrogel system, the blue light initiator was introduced to commence the cross-linking of the hydrogel in a friendly way. Bone components include inorganic calcium and phosphorus, which constitute 50%–70% of the human bone. Nanohydroxyapatite ($Ca_{10}(PO_4)_6(OH)_2$, nHA) provided nutrition for bone defects and showed good effects in bone repair [33,34]. Meanwhile, nHA has been proved to have tumor inhibition ability in recent years [35]. In addition, the nHA hybrid hydrogel is expected to supply a mimic ECM after osteosarcoma invasion and promote the repair of bone defects.

In this study, a GNRs/nHA hybrid hydrogel was designed *via* light-induced photopolymerization (Scheme 1A). Methacrylated gelatin (GelMA) and methacrylated chondroitin sulfate (CSMA) were selected as the hydrogel ingredients to form a biocompatible hydrogel. GNRs and nHA well dispersed in the hydrogel. The prepared GNRs/nHA hybrid GelMA/CSMA hydrogel was applied to eradicate the postoperative residual tumor by PTT as well as healing of the bone defect caused by the surgical resection of bone tumor (Scheme 1B). The outstanding properties of the GNRs/nHA hybrid GelMA/CSMA hydrogel are as follows: (1) the photothermal ability of hydrogel can induce the residual tumor apoptosis after surgery, and (2) the hybrid hydrogel occupies the region of the tissue defect region and helps bone regeneration, which was destroyed by osteosarcoma. It is believed that such a hybrid hydrogel in the bone tumor treatment has not yet been reported so far. A comprehensive characterization of the hybrid hydrogel system was conducted, and the research on the photothermal treatment of tumors and the repair of bone defects was systemically assessed *in vitro* and *in vivo*. This study reported a bifunctional hybrid hydrogel with the ability to prevent tumor recurrence and form good bone, which brings a new idea for the treatment of osteosarcoma and provides a useful reference for the field of complex disease.

2. Materials and methods

2.1. Materials

Acid tetrachloroaurate (III) trihydrate ($HAuCl_4{\cdot}3H_2O$) was purchased from Sinopharm Chemical Reagent Co. Ltd. (Shanghai, China). Cetyltrimethyl ammonium bromide (CTAB) was obtained from China National Medicines Corp., Ltd. (Beijing, China). Silver nitrate, and L (+)-ascorbic acid were purchased from Alfa Chemicals Ltd. (Bracknell, UK). Thiolated polyethylene glycol (Mw = 5000 KDa) was purchased from Sigma-Aldrich (St. Louis, MO, USA). In addition, GelMA, nHA, and lithium phenyl-2,4,6-trimethylbenzoylphosphinate (LAP) were obtained from Aladdin Industrial Corporation (Waukesha, WI, USA). Methacrylated chondroitin sulfate (CSMA) was obtained from StemEasy Biotech (Jiangyin, China). Moreover, LIVE/DEAD Cell Imaging Kit (Thermo

Fisher Scientific Inc., Waltham, MA, USA) was purchased from KeyGen BioTECH Co. Ltd. (Nanjing, China). Dulbecco's modified Eagle's medium and fetal bovine serum (FBS) were supplied by Gibco (Grand Island, NY, USA). The minimum essential medium eagle-alpha modification (α-MEM) was obtained from HyClone Laboratories Inc. (Tianjin, China). Alizarin Red Staining (ARS) was obtained from Beyotime Biotech Inc. (Jiangsu, China).

2.2. The preparation and characterization of GNRs

GNRs were synthesized through a conventional seed-mediated approach, which can be found in a previous study [11]. The surface of synthesized GNRs was coated with CTAB, which possess severe cell toxicity. Therefore, CTAB was replaced by thiolated PEG. Moreover, 200 mg of thiolated PEG in 32-mL aqueous water was added to GNRs with a 1-mg/mL concentration of gold (Au). The PEG/Au molar ratio was 0.20. The mixture was followed by gentle stirring for 24 h. Finally, the PEGylated GNRs were purified twice by centrifugation at 12,000 rpm for 10 min. The transmission electron microscopy (TEM) micrographs of GNRs were obtained on a Tecnai G^2 F20 S-TWIN TEM (FEI Co., Hillsboro, OR, USA) at an accelerated voltage of 120 kV. The absorption spectra of GNRs were tested by a PerkinElmer UV–Vis spectrophotometer (Lambda 35, Waltham, MA, USA).

2.3. The preparation and characterization of GNRs/nHA hybrid hydrogel

GelMA and CSMA were dissolved in water solution at 40% (w/v) and 20% (w/v), respectively. Solution A comprised a mixture of 70-μL GelMA and 60-μL CSMA. Subsequently, 2 mg/mL GNRs and 2 mg/mL nHA were sonicated for a while before use. Furthermore, 10 μL of GNRs and 10 μL of nHA were added to solution A, and the initiator LAP (0.5%, *w/v*, 20 μL) was added to the final solution. For hydrogel formation, 100 μL of suspension mixture was injected into a cylindrical silicone mold. A dental curing light was used to initiate hydrogel formation producing blue light at 420- to 480-nm wavelength and 1200- to 2000-mW/cm^2 power. After 2 min of exposure, the photopolymerized hydrogel was removed from the mold and immersed in Milli-Q aqueous water to eradicate residual monomers and initiators. The cross-section morphologies and elemental analysis of freeze-dried hydrogels were observed using a scanning electron microscopy (SEM) machine (JSM-5900LV, JEOL, Tokyo, Japan). The mechanical properties of wet hydrogels were determined by an Instron 5500 mechanical tester.

2.4. The photothermal ability of GNRs/nHA hybrid hydrogel

The GNRs/nHA hybrid hydrogel was irradiated by an 808-nm laser with a different power density (0.08, 0.56, and 0.99 W/cm^2) for 5 min. Blank hydrogel without GNRs was used as the control sample. Temperature changes were recorded timely, and NIR images were taken by a Fluke Ti32 Infrared (IR) thermal camera system (Fluke, Everett, WA, USA). Furthermore, the tissue penetration on the photothermal ability of hybrid hydrogel was assessed on *ex vivo* pork skin and bone tissues.

2.5. The viability assay of tumor cells after photothermal treatment

For tumor cell viability measurements, K7M2wt cells (a mouse bone tumor cell line) were plated into 96-well plates (5.0×10^3 cells/well) and allowed to adhere to the plate surface before the addition of hybrid hydrogel. The cells were then irradiated by laser with a different power density (0.08, 0.56, and 0.99 W/cm^2) for 5 min. After the hydrogel was moved out, the cells were stained using LIVE/DEAD Cell Imaging Kit for 30 min. The cells were then washed using phosphate-buffered saline (PBS), and imaged with fluorescence microscopy (Leica Microsystem Inc., Wetzlar, Germany). Consequently, the cell survival percentage was determined for quantitatively analysis.

2.6. In vitro cytotoxicity assay

The leachates were extracted from the hydrogel in the cell medium for 24 h to study hydrogel cytotoxicity. NIH3T3 cells (a mouse embryonic fibroblast cell line) and K7M2wt cells were seeded into a 96-well plate (5×10^3 cells/well, 100 μL) for overnight adhesion. Subsequently, the old cell medium was changed to leachates with different concentrations. Untreated cells in the growth media were used as blank control. After 24 h of incubation, cell viability was determined by the methylthiazolydiphenyl-tetrazolium bromide (MTT) assay.

2.7. The culture of MSCs and osteogenic evaluation

The hybrid hydrogels were disinfected overnight with 75% ethanol and washed with sterile PBS. The hydrogels can be used to cell study after they are balanced with the cell medium. The MSCs were isolated from the bone marrow of newborn mice at 3 days old. They were expanded in standard growth α-MEM medium with 10% FBS, and incubated in a 5% CO_2 atmosphere. MSCs were cultured to the third passage and trypsinized to incubate on the hydrogel. The cells on hydrogels were incubated for 1, 3, and 5 days to observe their attachment and proliferation. Samples with cells were fixed in 2.5% glutaraldehyde for 30 min and dehydrated by freeze-drying to study the morphology of the cells and their adhesion using SEM. Meanwhile, cell proliferation was measured using MTT assay.

The osteogenic potential evaluation was conducted with the ECM mineralization by ARS. After the MSCs adhered to the hydrogel, the medium was changed to an osteoinductive medium containing 10% FBS, 1% penicillin–streptomycin, 50 μg/mL ascorbic acid, 10 mM sodium β-glycerophosphate, and 100 nM dexamethasone. Consequently, the medium was refreshed every 2 days. After incubation for 14 days, cells were washed and fixed to stain with 0.2% ARS for 30 min. The mineralized matrix stain was dissolved in cetylpyridinium chloride for quantification analysis.

2.8. In vivo biocompatibility and degradation of the hybrid hydrogel

In vivo biocompatibility and degradation tests were explored by implanting the hydrogel into the subcutaneous tissues of BALB/c mice (~20 g). Implanted subcutaneously into the back of the mice were 200-μL hydrogels. The mice were sacrificed by cervical dislocation at 1, 2, and 4 weeks. The implanted regions were carefully opened, and the remaining gels were photographed. The surrounding tissues were surgically removed and subjected to hematoxylin and eosin (H&E) staining for study tissue responses.

2.9. In vivo postoperative PTT and bone repair

A tumor implantation method was used to construct the tumor model for high tumor formation rate because the bone tumor model in mice was relatively difficult to build. All the animal procedures were performed according to the guidelines approved by Sichuan University. Female BALB/c mice (3 weeks old) were purchased from Beijing HFK Bioscience Co. Ltd. (Beijing, China). Moreover, K7M2wt cells (1.0×10^6) were subcutaneously injected into the left leg of the mice. When the diameter of the tumor reached ~5 mm, the mice were sacrificed, and their tumors were removed and cut into small fragments. The tumor mass with diameter of ~2 mm was separately implanted in the site near the tibia, which was grounded to damage the bone membrane for tumor invasion. Consequently, the bone tumor model was built after 1 week. Tumor-bearing mice were then randomly separated into four groups (total number = 20, $n = 5$). After the mice were anesthetized, the tumor was surgically removed. However, the remaining tumor was left around the tibia. The GNRs/nHA hybrid hydrogel (100 μL) was implanted *in situ*, and the incision was sutured. Subsequently, the mice were irradiated with the 808-nm laser for 5 min (0.99 W/cm^2). The temperature

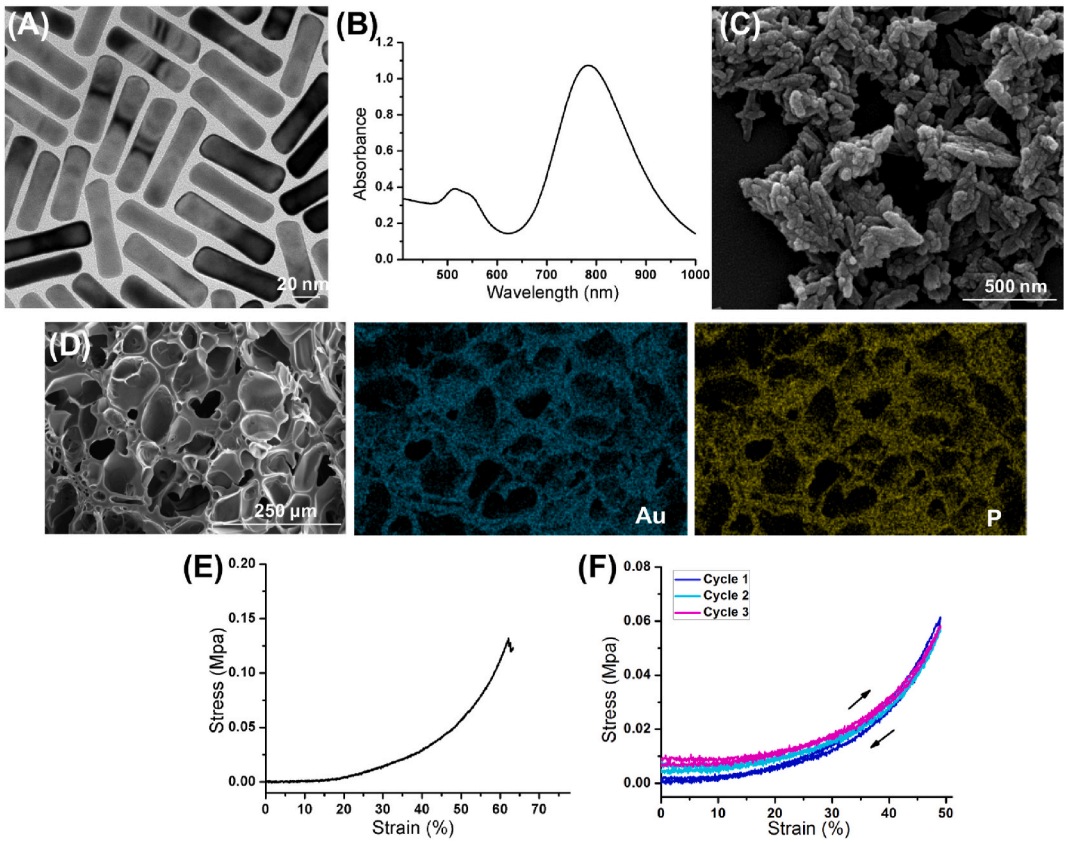

Fig. 1. **(A)** The TEM and **(B)** UV–Vis absorption curve of PEGylated GNRs; **(C)** the SEM image of nHA; **(D)** the SEM image and element mapping of the cross section of GNRs/nHA hybrid hydrogel; **(E)** the compressive stress curve of GNRs/nHA hybrid hydrogel as a function of strain; and **(F)** fatigue-resistance hydrogel with three successive loading–unloading cycles of compression.

distribution images of the leg tissues were recorded during the irradiation period. The mice were then weighed, and their tumor sizes were measured every 2 days. Considering that the bone tumor was close to the skin, the tumor volume can be measured with a digital caliper and calculated as volume = (tumor length) × (tumor width)^2/2. The life span of the mice was observed. Another batch of mice was sacrificed after treatment for 2 weeks. Their tibias were removed for micro-computed tomography (micro-CT) scan and H&E staining. Their heart, lung, liver, spleen, kidney, and recurrent tumor were subjected to H&E staining.

2.10. Statistical analysis

The statistical analysis was performed using SPSS 15.0 software (Chicago, IL, USA). Statistical comparisons were identified by a Student's *t*-test. Statistical significance was considered when the value of P was less than 0.05.

3. Results and discussion

3.1. The synthesis and characterization of GNRs/nHA hybrid hydrogel

The prepared PEGylated GNRs have a uniform morphology in the TEM image (Fig. 1A), which possessed a length and width of ~48 and ~12 nm, respectively. PEGylated GNRs were biocompatible after CTAB eradication. The GNRs exhibited strong absorbance in the NIR region with a peak at ~808 nm (Fig. 1B). The obtained nHA presented a spindle-like morphology in nanodiameter (Fig. 1C). The GNRs/nHA hybrid hydrogel was then prepared by photo-crosslinking method (Fig. S1), which was mild and quick. GelMA and CSMA monomers were the main hydrogel matrix and can form a compatible hydrogel in 2 min with blue light irradiation. The freeze-dried hydrogel possessed a porous structure, and its mean pore size was ~76 μm (Fig. 1D). From the element mapping analysis, the cross section of GNRs/nHA hybrid hydrogel showed the coexistence of Au and phosphorus (P), indicating that the GNRs and nHA were homogeneously distributed in the hydrogel.

The mechanical property was important to maintain the structure of hydrogels in their work position. The mechanical performance of GNRs/nHA hybrid hydrogel was evaluated by an Instron mechanical tester. The elastic modulus of the hydrogel was 0.67 Mpa, and the ultimate stress of the crack point was at 62% compression (Fig. 1E). Furthermore, the fatigue resistance property of the hydrogel has been tested. The hybrid hydrogel kept its integrity after three successive loading–unloading compression cycles (Fig. 1F).

3.2. The photothermal ability of GNRs/nHA hybrid hydrogel

The photothermal ability is important for tumor therapy. The GNRs in the hybrid hydrogel for the photothermal effect response has been introduced in this study. Real-time thermal images showed changing colors in the center and the surrounding region of the hydrogel as time went on (Fig. 2A). From the results of the heating curves, the blank hydrogel without GNRs showed no temperature rise under NIR light irradiation. On the contrary, the GNRs/nHA hybrid hydrogel displayed regulated high temperatures in response to different power densities of the NIR laser irradiation. The temperature increased to 35.0 °C, 47.1 °C and 57.6 °C under the irradiation power densities of 0.08, 0.56, and 0.99 W/cm^2, respectively (Fig. 2B). The results indicated a good photothermal performance of GNRs/nHA hybrid hydrogel.

Pork skin and bone tissues were utilized to investigate the heating penetration depth to better understand the heating transfer efficiency of

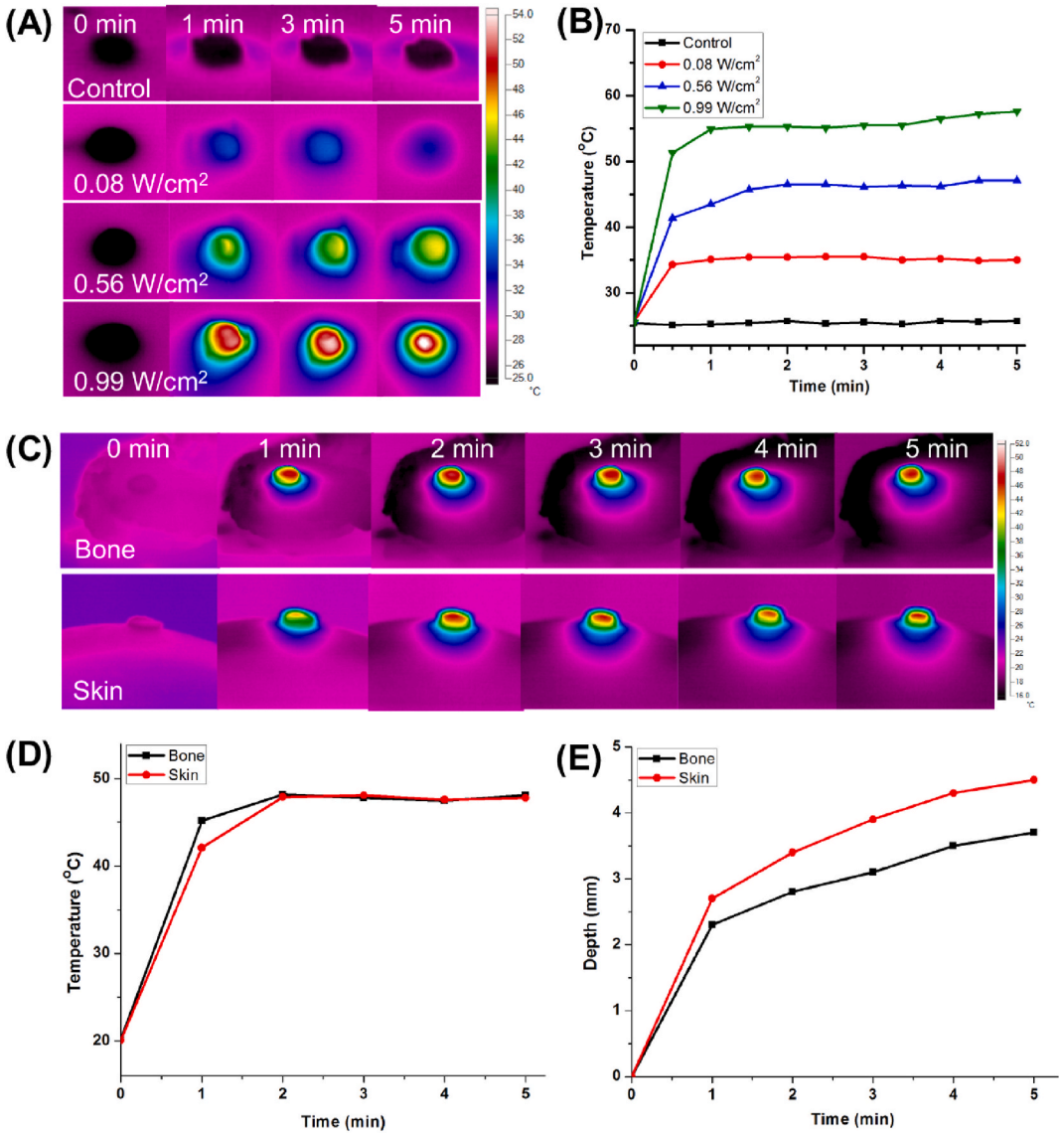

Fig. 2. **(A)** The real-time thermal images and **(B)** the photothermal curves of the control group (blank hydrogel under NIR light irradiation at the power density of 0.99 W/cm^2) and GNRs/nHA hybrid hydrogel with a different power density of irradiation; **(C)** Heating transfer efficacy images, and **(D)** curves at the center temperature of hydrogels, and **(E)** heating penetration depths of GNRs/nHA hybrid hydrogel on pock bone and skin with 808-nm laser irradiation within 5 min.

the GNRs/nHA hybrid hydrogel. Fig. 2C shows both two kinds of tissues depicting the heating diffusion along with time. The center temperature of the hydrogel in the two groups showed no significant difference (Fig. 2D). However, bone tissue displayed a lower heating diffusion region compared with skin tissue during the irradiation duration. The heating penetration depths in bone and skin were approximately 3.7 and 4.5 mm (Fig. 2E), respectively. From the results, it can be concluded that the center of heating in hydrogels was almost the same and different heating transfer efficiency existed in different tissues. Therefore, the idea that the photothermal treatment of bone tumor postoperatively removes the majority of the tumor tissue was obtained, considering that the limited heating transfer efficiency cannot defend the whole tumor region. Moreover, the postoperative therapy strategy is close to clinical treatment method.

3.3. *Photothermal effects of GNRs/nHA hybrid hydrogel on bone tumor cells*

The *in vitro* photothermal effect of GNRs/nHA hybrid hydrogel was performed on the viability of K7M2wt osteosarcoma cells. A different power density was explored on the wet hydrogel in temperature changes for tumor cell survival. Moreover, Fig. 3A shows that the green and red cells represented the live and dead cells, respectively. The cells with increasing laser power density were dead. The viabilities of tumor cells were 99.3%, 73.0% and 1.2% in groups of 0.08, 0.56, 0.99 W/cm^2, respectively (Fig. 3B). The temperature elevation of the hydrogels in the cell medium was increased to 37.5 °C, 46.0 °C and 59.9 °C after laser irradiation for 5 min with different power densities (Fig. 3C). The inset circle images shown in Fig. 3C are the IR images of the hydrogel in plates. The relative hyperthermia of >50 °C for 5 min is sufficient to destroy the tumor cells [36]. Although the temperature was 59.9 °C under the power density of 0.99 W/cm^2, the penetration medium in the cell study was different from *in vivo* studies. Moreover, water easily penetrates and spreads heat than the animal's tissues (e.g. skin, tumor, and bone). Therefore, the power density of 0.99 W/cm^2 was selected in the following *in vivo* tumor treatment according to the photothermal capability of GNRs/nHA hybrid hydrogel in the cell study.

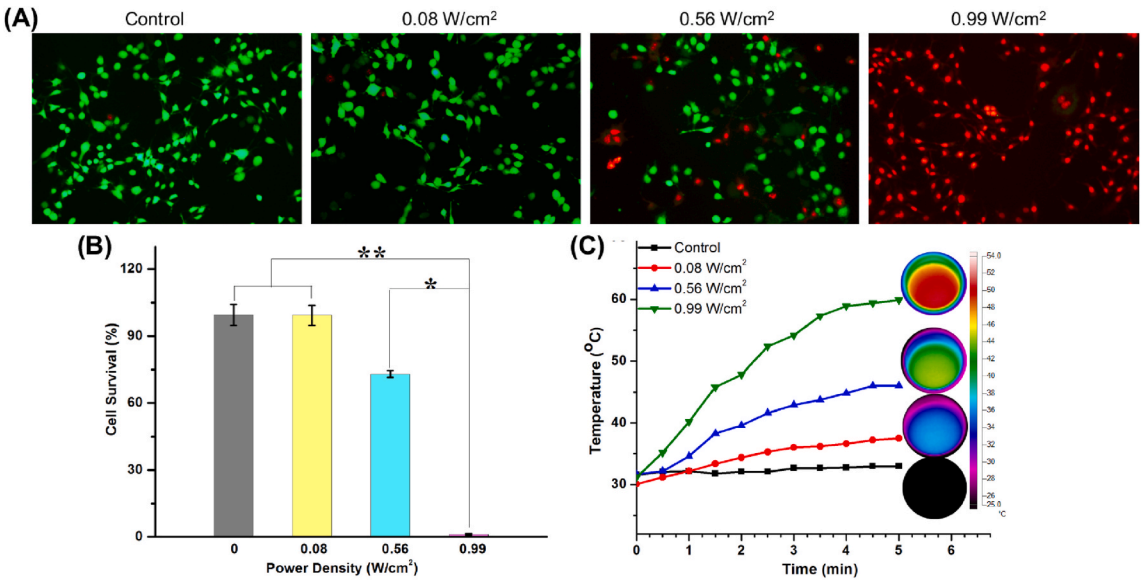

Fig. 3. **(A)** The fluorescent images of K7M2wt bone tumor cells stained with calcein AM (*green* live cells) and PI (*red* dead cells; magnification × 200); **(B)** relative viability of bone tumor cells in blank and hybrid hydrogels with different power densities treatment (*P < 0.05, **P < 0.01); and **(C)** heating curves of the wet hydrogels in plates with cell medium (the inset circle images were the IR pictures of the hydrogel in plates).

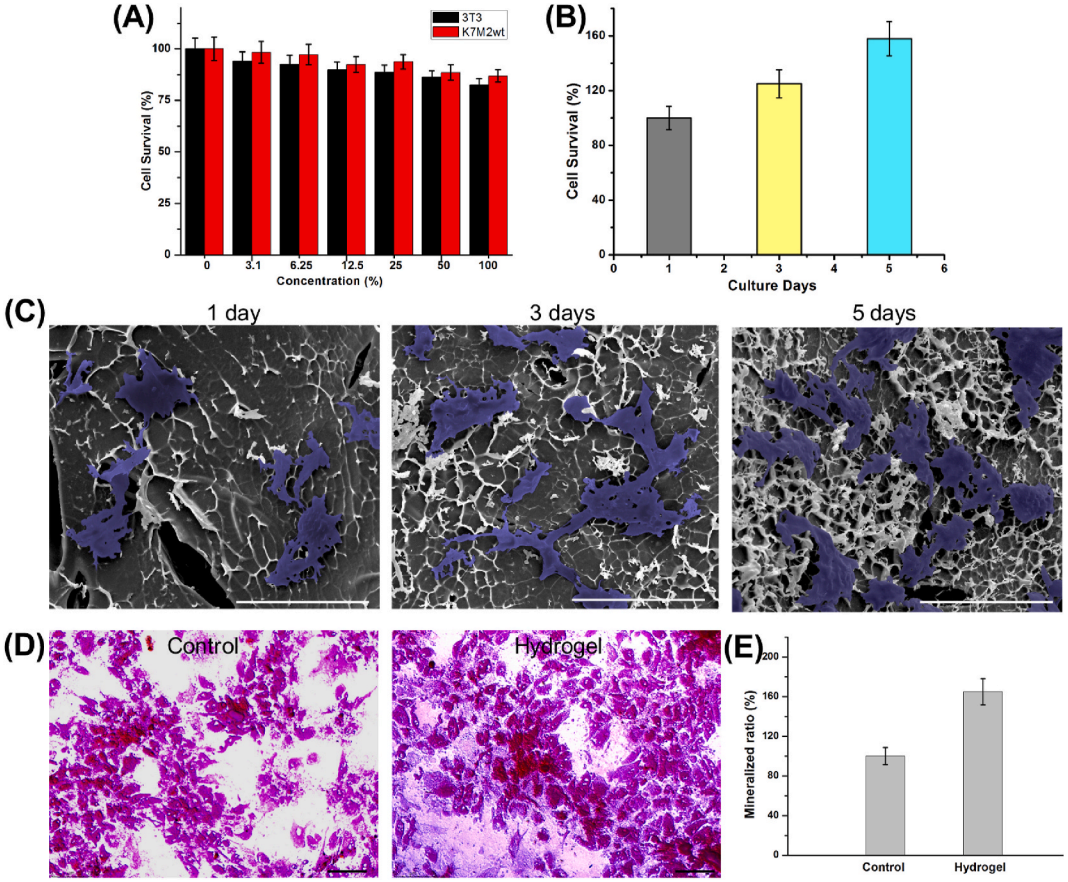

Fig. 4. **(A)** The cytocompatibility of GNRs/nHA hybrid hydrogel; **(B)** the cell survival ratios cultured with GNRs/nHA hybrid hydrogel along with the incubation days; **(C)** the SEM images of MSCs adhered to GNRs/nHA hybrid hydrogel and their growth in 1, 3, and 5 days (the cells were marked in *blue*; *scale bar* 200 μm); **(D)** the optical photos of ARS (*scale bar* 75 μm), and **(E)** mineralized ratios in the control and hydrogel groups.

3.4. *In vitro* cell cytotoxicity and MSCs growth

The cell cytotoxicity of GNRs/nHA hybrid hydrogel was evaluated by cell survival assay using 3T3 cells and K7M2wt cells. Fig. 4A exhibits the cell viability in the presence of GNRs/nHA hybrid hydrogel leachates with different concentrations. The cell survival rate was compared with

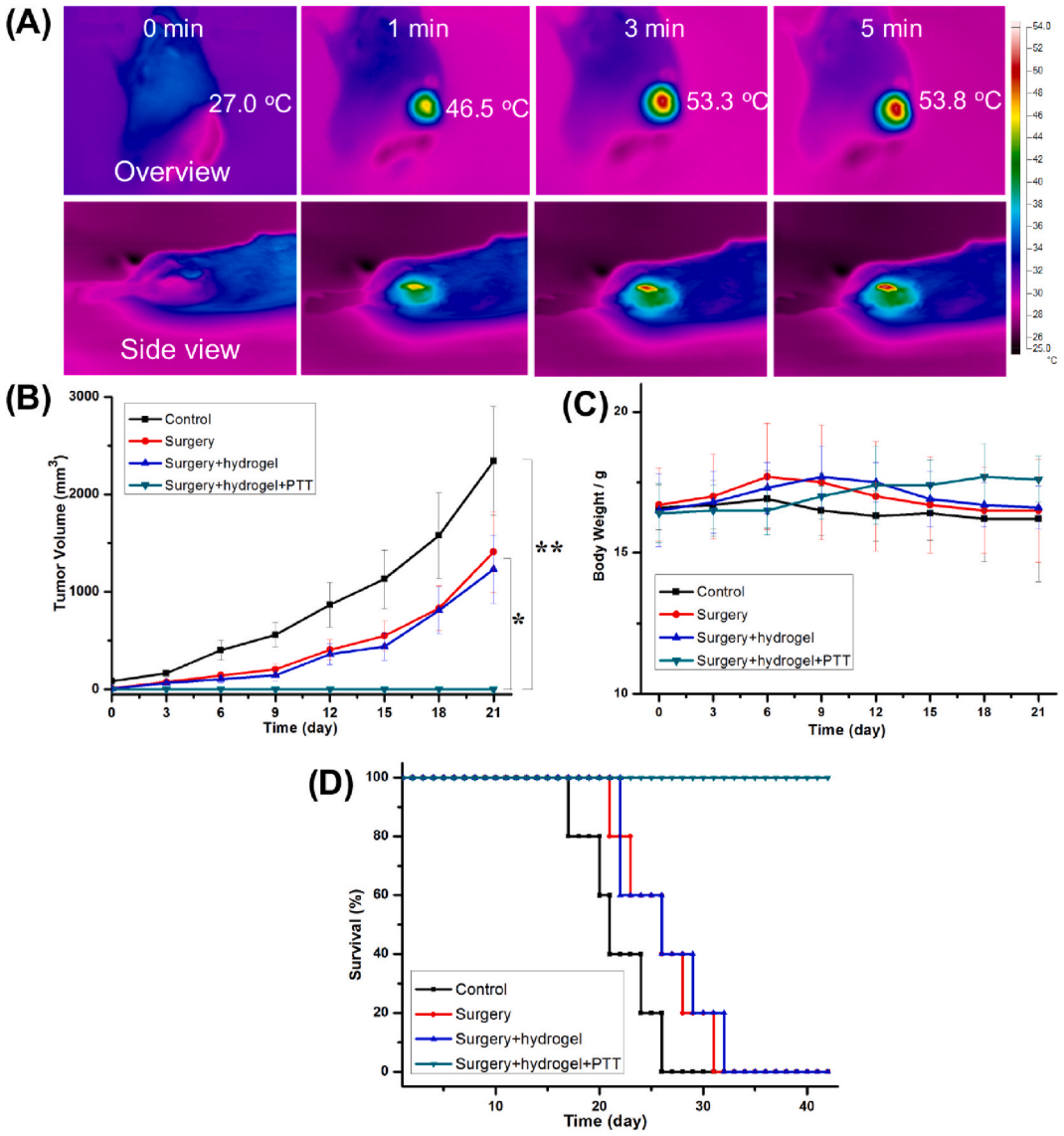

Fig. 5. **(A)** The infrared thermal images of tumor-bearing mice were taken on overview and side view after implantation with GNRs/nHA hybrid hydrogel exposed to 808-nm laser irradiation. **(B)** The changes in tumor volume (*P < 0.05, **P < 0.01), **(C)** body weights, and **(D)** survival rates of mice in each group.

that of the control group, whose cells had been cultured in cell medium without any other additives. Consequently, both 3T3 and K7M2wt cell viability decreased slowly with the increase of the hydrogel leachates concentration. Fortunately, cell viability was assessed as > 80% even at a relatively high concentration. Therefore, the GNRs/nHA hybrid hydrogel prepared in this study possessed good cell compatibility.

Subsequently, the growth of MSCs was evaluated by the MTT assay and SEM analysis. The cell survival ratios were detected to quantitatively analyze cell viability. Fig. 4B shows that the cell viability increased at 25% and 58% after incubation for 3 and 5 days, respectively. The incubated MSCs on hydrogels were denoted as blue region for easy distinction in the cells' morphology analysis shown in the SEM images in Fig. 4C. The MSCs adhered and anchored on the GNRs/nHA hybrid hydrogel on the first day of incubation. In addition, the MSCs spread and proliferated on the hydrogel well along with the culture time. They can grow on the hydrogel in a good state. The results indicated that the viability or shapes of MSCs maintained a good condition cultured on the GNRs/nHA hybrid hydrogel.

The ECM formation was assessed using ARS cultured for 14 days to evaluate the osteogenic differentiation of MSCs. The hydrogel group presented a higher density of mineralized nodules compared with the control group without hydrogel (Fig. 4D). Meanwhile, the amount of mineralized matrix was determined (Fig. 4E). The MSCs in the hydrogel group produced 65% higher mineralized ECM than those in the control group, indicating that the hybrid hydrogel promoted the osteogenic differentiation of MSCs. The addition of nHA in the hydrogel may mimic the natural structure of ECM in the bone, resulting in promoted osteogenic cell proliferation, differentiation, and mineralization.

3.5. *In vivo biocompatibility and degradation of GNRs/nHA hybrid hydrogel*

The biocompatibility and degradation of GNRs/nHA hybrid hydrogel were investigated by implanting subcutaneously at the back of BALB/c mice. From visual observation, the hydrogel gradually degraded with time (Fig. S2A). From H&E staining (Fig. S2B), some macrophages and lymphocytes immigrated into the connective tissue around the hydrogel in the first week. The existing inflammatory cells imply a slight inflammatory response. Subsequently, the number of macrophages and lymphocytes gradually reduced at 2 and 4 weeks. Therefore, the GNRs/nHA hybrid hydrogel is biodegradable and possesses acceptable biocompatibility for further applications.

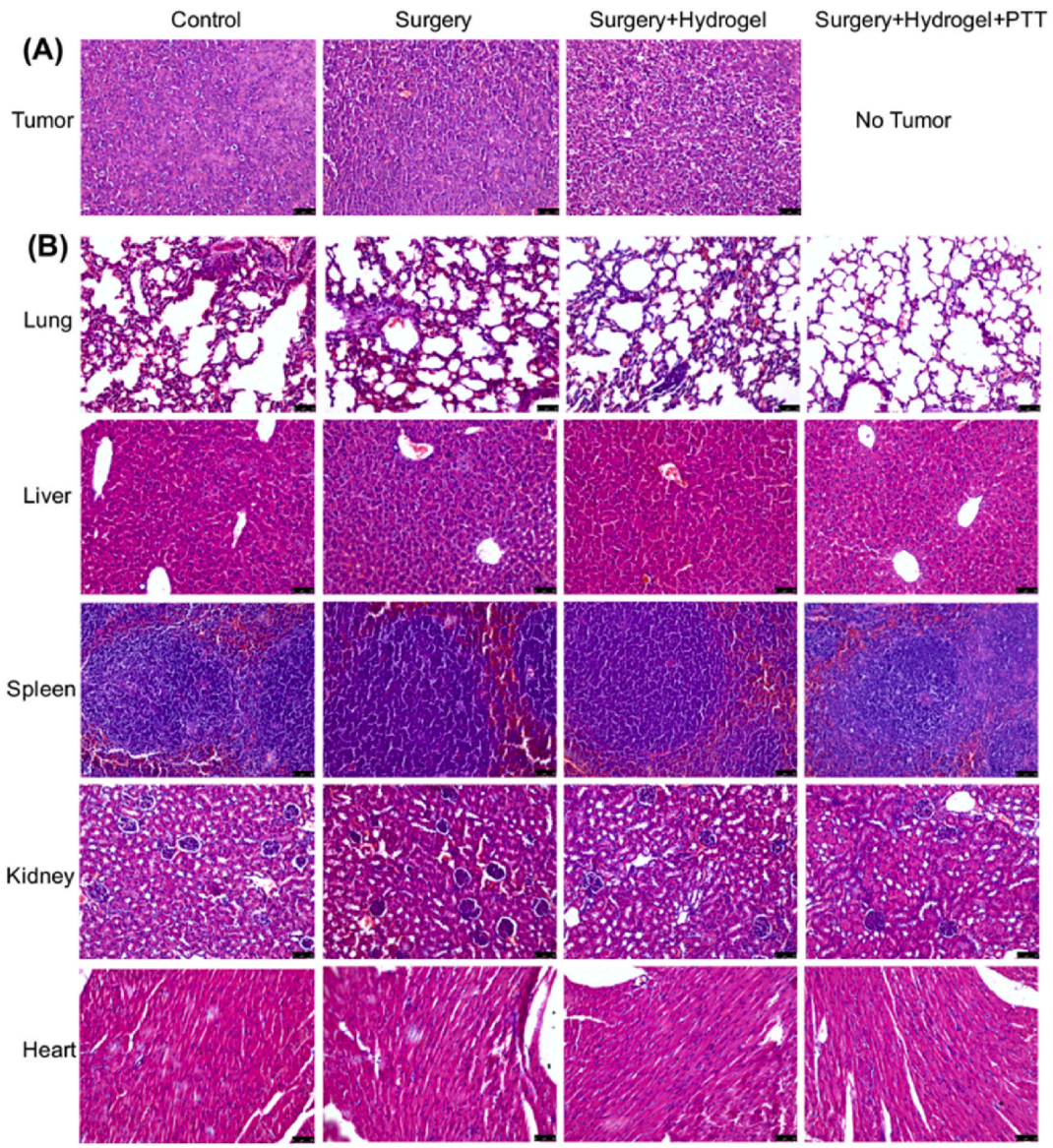

Fig. 6. H&E staining of **(A)** tumors and **(B)** main organs of the different groups of mice after treatment for 2 weeks (*scale bar* 50 μm).

3.6. In vivo bone tumor therapy of GNRs/nHA hybrid hydrogel

The mice were randomly divided into four groups (control, surgery, surgery + hydrogel, and surgery + hydrogel + PTT groups). Two batches of mice study were constructed. One batch was used for observation of the bone repair after tumor therapy, and one batch was used for the measurement of tumor volumes, body weight, and life span. In the experiments, the bone tumor model was successfully built by implantation of tumor fragments, which can be found in the micro-CT reconstruction (Fig. S3A). The bone tumor has invaded the tibia of the mice. The surgery process is presented in Figs. S3B–E. The removal of the tumor tissue was tried, but some residual tumor was difficult to eradicate. The GNRs/nHA hybrid hydrogel was then implanted for photothermal treatment to destroy the residual tumor. The IR thermal images of tumor-bearing mice were taken at different time points exposed to 808-nm laser irradiation with a power density of 0.99 W/cm^2 (Fig. 5A). From the overview side, the center temperature of the residual bone tumor containing hybrid hydrogel quickly increased and was maintained at ~53.8 °C, which is beneficial for destroying the residual tumor tissues. Meanwhile, the surrounding region of the hydrogel was ~40 °C from the side view pictures due to the limited irradiation region of the laser and penetration depth of the heat. The mild heat temperature was safe to the normal tissues and may simulate MSCs in osteogenesis differentiation [37,38]. The results indicated that PTT was capable of minimal invasiveness to the body and selective tumor destruction without damaging the surrounding healthy tissues.

Tumor-bearing mice were kept for systemic evaluation of tumor growth (Fig. 5B), body weight (Fig. 5C), and survival rate (Fig. 5D). In the control group, the tumors in the mice grew very quickly and mice mortality was 20% after 18 days of tumor invasion. In the surgery and surgery + hydrogel groups, the tumors regrew on the basis of the live residual tumor and no significant difference was noted in the tumor volumes. In addition, their tumor growth was delayed to some extent by surgery compared with that of the control group. In the surgery + hydrogel + PTT group, the postoperative residual tumor tissues were cured by PTT with no further recurrence. In bodyweight detection, 1 week may be a watershed. From this time point, the body masses of mice in the control, surgery, and surgery + hydrogel groups decreased. On the contrary, the mice in the surgery + hydrogel + PTT group grew well with increased body weight. Fig. 5D shows the survival rate of the mice in each group evaluated at 6 weeks. The control group first appeared with mice mortality, and all gradually followed dead within 26 days.

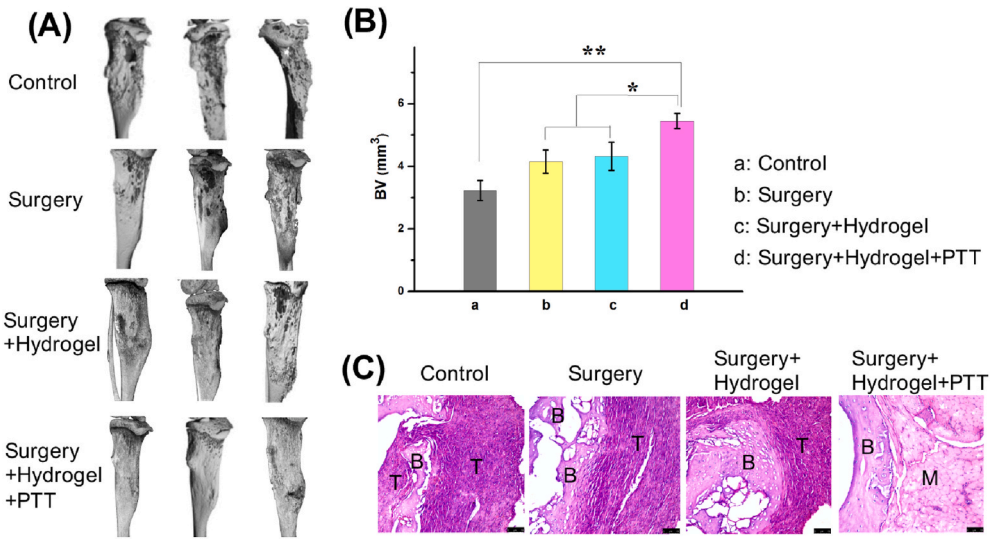

Fig. 7. **(A)** The micro-CT reconstruction in each group of mice after treatment for 2 weeks; **(B)** The bone volume (BV) parameter in each group of mice (*P < 0.05, **P < 0.01); **(C)** H&E staining images of the tibia bone tumor interface in different groups (*B* bone, *T* tumor, *M* muscle; *scale bar* 50 μm).

The surgery and surgery + hydrogel groups showed a similar survival rate, and their life span was prolonged for ~1 week with the removal of the majority of the tumor. Fortunately, the mice in the surgery + hydrogel + PTT group were alive during the observation period, and their tibia bone defect repair was assessed on follow-up.

In another batch of *in vivo* experiments, the mice were sacrificed at 2 weeks postoperatively to analyze tumor invasion and bone. The mice images in different groups are shown in Fig. S4. Their *ex vivo* tumors and main organs were stained with H&E and the tibia tissues were used for micro-CT reconstruction. As shown in Fig. 6A, the bone tumor cells in the control, surgery, and surgery + hydrogel groups were densely arranged. Fortunately, no tumor existed in their legs after postoperative surgery and PTT in the surgery + hydrogel + PTT group. From the staining of main organs (Fig. 6B), no tumor metastasis was found in the surgery + hydrogel + PTT group. However, small tumor nodules in the lungs and some points of pulmonary bleeding were found in the other three groups. The results suggest that the tumors quickly grew in these groups and invaded the lungs through the circulatory system in a short duration.

In the micro-CT observation (Fig. 7A), the tibia in the control group was invaded inside by a tumor. Moreover, the tumor-induced bone erosion in surgery and surgery + hydrogel groups. Although the surgery can destroy tumor mass, the residual tumor was regrown with a high rate of recurrence, leading to an aggressive bone defect. Fortunately, the mice in the surgery + hydrogel + PTT group showed a better therapeutic effect with the regenerated bone. The surrounding residual bone tumor was destroyed by PTT, and the bone defect regeneration was promoted by the hybrid hydrogel. Bone histomorphometrics in each group was analyzed (Fig. 7B). The bone volume data in the surgery + hydrogel + PTT group were significantly higher than those in other groups. Furthermore, H&E staining was performed to observe tumor invasion (Fig. 7C). Moreover, the tumor involved in the osteolysis in the control groups was more obvious and aggressive. Tumor regrowth was inhibited, and the defective tibia was gradually repaired with the hybrid GNRs/nHA hydrogel treatment. The repaired bone section was not in an integrated form within 2 weeks, and the defective muscle region needed a longer time to connect well. Overall, the hybrid GNRs/nHA hydrogel possessed the dual function of effectively destroying the residual tumor cells and healing the bone defect after osteosarcoma surgical resection. Furthermore, this bifunctional hydrogel system gave an important reference in tumor-induced bone defect repair.

4. Conclusions

Considering the clinical needs, disease characteristics, and existing problems, this study constructed a novel type of bifunctional hybrid hydrogel. The hybrid hydrogel platform has advantages as below (1) the introduction of GNRs was suitable for the photothermal treatment of residual tumor cells after surgery to prevent tumor recurrence, and (2) the nHA hybrid in the hydrogel helped repair bone defects invaded by tumor. This composite hydrogel combines the dual functions of tumor photothermal treatment and bone defect repair. This difunctional hydrogel system platform was suitable not only for osteosarcoma, but also for the treatment of complex diseases such as maxillofacial defects caused by oral cancer, and bone metastases of malignant tumors. The development and research of this new type of hybrid scaffolds will bring new hope for malignant complex diseases and provide with new vitality for the development of future medicine.

CRediT authorship contribution statement

Jinfeng Liao: Investigation, Methodology, Data curation, Writing - original draft. **Kun Shi:** Investigation, Methodology. **Yanpeng Jia:** Investigation, Methodology. **Yanting Wu:** Methodology, Data curation. **Zhiyong Qian:** Supervision, Writing - review & editing.

Declaration of competing interest

There is no conflict of interest for all the authors.

Acknowledgments

This work was financially supported by the National Key Research and Development Program of China (2017YFC1103500, 2017YFC1103502), the National Natural Science Foundation (31972925, 31771096, 31930067, 31525009), 1·3·5 project for disciplines of excellence, West China Hospital, Sichuan University (ZYGD18002), Sichuan Science and Technology Program (2020YJ0065), Sichuan University Spark Project (2018SCUH0029), State Key Laboratory of Oral Diseases Foundation (SKLOD202016).

Appendix A. Supplementary data

Supplementary data to this article can be found online at https://doi.org/10.1016/j.bioactmat.2021.01.006.

References

[1] K.N. Weibaecher, T.A. Guise, L.K. McCauley, Cancer to bone: a fatal attraction, Nat. Rev. Canc. 11 (2011) 411–425, https://doi.org/10.1038/nrc3055.

[2] N. Rainusso, L.L. Wang, J.T. Yustein, The adolescent and young adult with cancer: state of the art-bone tumors, Curr. Oncol. Rep. 15 (2013) 296–307, https://doi.org/10.1007/s11912-013-0321-9.

[3] E. Simpson, H.L. Brown, Understanding osteosarcomas, J. Am. Acad. Phys. 31 (2018) 15–19, https://doi.org/10.1097/01.JAA.000541477.24116.8d.

[4] D. Gianferante, L. Mirabello, S. Savage, Germline and somatic genetics of osteosarcoma-connecting aetiology, biology and therapy, Nat. Rev. Endocrinol. 13 (2017) 480–491, https://doi.org/10.1038/nrendo.2017.16.

[5] S.E. Ballatori, P.W. Hinds, Osteosarcoma: prognosis plateau warrants retinoblastoma pathway targeted therapy, Signal Transduct. Tar. 1 (2016) 16001, https://doi.org/10.1038/sigtrans.2016.1.

[6] Y. Liu, P. Bhattarai, Z. Dai, X. Chen, Photothermal therapy and photoacoustic imaging via nanotheranostics in fighting cancer, Chem. Soc. Rev. 48 (2019) 2053–2108, https://doi.org/10.1039/c8cs00618k.

[7] S. Pan, J. Yin, L. Yu, C. Zhang, Y. Zhu, Y. Gao, Y. Chen, 2D MXene-integrated 3D-printing scaffolds for augmented osteosarcoma phototherapy and accelerated tissue reconstruction, Adv. Sci. 7 (2020) 1901511, https://doi.org/10.1002/advs.201901511.

[8] W. Zhang, J. Gu, K. Li, J. Zhao, H. Ma, C. Wu, C. Zhang, Y. Xie, F. Yang, X. Zheng, A hydrogenated black TiO_2 coating with excellent effects for photothermal of bone tumor and bone regeneration, Mater. Sci. Eng. C 102 (2019) 458–470, https://doi.org/10.1016/j.msec.2019.04.025.

[9] L. Wang, N.J. Long, L. Li, M. Li, J. Cao, Y. Zhang, Q. Zhang, S. Xu, Z. Yang, C. Mao, M. Peng, Multi-functional bismuth-doped bioglasses: combining bioactivity and photothermal response for bone tumor treatment and tissue repair, Light Sci. Appl. 7 (2018) 1, https://doi.org/10.1038/s41377-018-0007-z.

[10] Y. Xue, W. Niu, M. Wang, M. Chen, Y. Guo, B. Lei, Engineering a biodegradable multifunctional antibacterial bioactive nanosystem for enhancing tumor photothermo-chemotherapy and bone regeneration, ACS Nano 14 (2020) 442–453, https://doi.org/10.1021/acsnano.9b06145.

[11] J. Liao, W. Li, J. Peng, Q. Yang, H. Li, Y. Wei, X. Zhang, Z. Qian, Combined cancer photothermal-chemotherapy based on doxorubicin/gold nanorod-loaded polymersomes, Theranostics 5 (2015) 345–356, https://doi.org/10.7150/thno.10731.

[12] A.R. Rastinehad, H. Anastos, E. Wajswol, J.S. Winoker, J.P. Sfakianos, S. K. Doppalapudi, M.R. Carrick, C.J. Knauer, B. Taouli, S.C. Lewis, A.K. Tewari, J. A. Schwartz, S.E. Canfield, A.K. George, J.L. West, N.J. Halas, Gold nanoshell-localized photothermal ablation of prostate tumors in a clinical pilot device study, P. Natl. Acad. Sci. USA 116 (2019) 18590–18596, https://doi.org/10.1073/pnas.1906929116.

[13] X. Wang, T. Li, H. Ma, D. Zhai, C. Jiang, J. Chang, J. Wang, C. Wu, A 3D-printed scaffold with MoS_2 nanosheets for tumor therapy and tissue engineering, NPG Asia Mater. 9 (2017) e376, https://doi.org/10.1038/am.2017.47.

[14] W. Dang, T. Li, B. Li, H. Ma, D. Zhai, X. Wang, J. Chang, Y. Xiao, J. Wang, C. Wu, A biofunctional scaffold with $CuFeSe_2$ nanocrystals for tumor therapy and bone reconstruction, Biomaterials 160 (2018) 92–106, https://doi.org/10.1016/j.biomaterials.2017.11.020.

[15] H. Ma, J. Luo, Z. Sun, L. Xia, M. Shi, M. Liu, J. Chang, C. Wu, 3D printing of biomaterial with mussel-inspired nanostructures for tumor therapy and tissue regeneration, Biomaterials 11 (2016) 138–148, https://doi.org/10.1016/j.biomaterials.2016.10.005.

[16] Y. Hao, Y.W. Chen, X.L. He, F. Yang, R.X. Han, C.L. Yang, W. Li, Z.Y. Qian, Near-infrared responsive 5-fluorouracil and indocyanine green loaded MPEG-PCL nanoparticles integrated with dissolvable microneedle for skin cancer therapy, Bioactive Mater. 5 (2020) 542–552, https://doi.org/10.1016/j.bioactmat.2020.04002.

[17] G.L. Koons, M. Diba, A.G. Mikos, Materials design for bone-tissue engineering, Nat. Rev. 5 (2020) 584–603, https://doi.org/10.1038/s41578-020-0204-2.

[18] K. Zhang, Z. Jia, B. Yang, Q. Feng, X. Xu, W. Yuan, X. Li, X. Chen, L. Duan, D. Wang, L. Bian, Adaptable hydrogels mediate cofactor-assisted activation of biomarker-responsive drug delivery via positive feedback for enhanced tissue engineering, Adv. Sci. (2018) 180875, https://doi.org/10.1002/advs.201800875.

[19] D.K. Khajuria, V.B. Kumar, D. Gigi, A. Gedanken, D. Karasik, Accelerated bone regeneration by nitrogen-doped carbon dots functionalized with hydroxyapatite nanoparticles, ACS Appl. Mater. Interfaces 10 (2018) 19373–19383, https://doi.org/10.1021/acsami.8b02792.

[20] X. Wang, J. Shao, M.A.E. Raouf, H. Xie, H. Huang, H. Wang, P.K. Chu, X.-F. Yu, Y. Yang, A.M. AbdEI-Aal, N.H.M. Mekkawy, R.J. Miron, Y. Zhang, Near-infrared light-triggered drug delivery system based on black phosphorus for in vivo bone regeneration, Biomaterials 179 (2018) 164–174, https://doi.org/10.1016/j.biomaterials.2018.06.039.

[21] Y. Li, Y. Xiao, C. Liu, The horizon of materiobiology: a perspective on material-guide cell behaviors and tissue engineering, Chem. Rev. 117 (2017) 4376–4421, https://doi.org/10.1021/acs.chemrev.6b00654.

[22] C. Yang, Z. Huan, X. Wang, C. Wu, J. Chang, 3D printed Fe scaffolds with HA nanocoating for bone regeneration, ACS Biomater. Sci. Eng. 4 (2018) 608–616, https://doi.org/10.1021/acsbiomaterials.7b00885.

[23] T. Xu, H. Yang, D. Yang, Z.Z. Yu, Polylactic acid nanofiber scaffold decorated with chitosan islandlike topography for bone tissue engineering, ACS Appl. Mater. Interfaces 9 (2017) 21094–21104, https://doi.org/10.1021/acsami.7b01176.

[24] Y. Deng, X. Shi, Y. Chem, W. Yang, Y. Ma, X.-L. Shi, P. Song, M.S. Dargusch, Z.-G. Chen, Bacteria-triggered pH-responsive osteopotentiating coating on 3D-printed polyetheretherketone scaffolds for infective bone defect repair, Ind. Eng. Chem. Res. 59 (2020) 12123–12135. https://pubs.acs.org/doi/10.1021/acs.iecr.0c02107.

[25] J.Z. Yang, Y.S. Zhang, K. Yue, A. Khademhosseini, Cell-laden hydrogels for osteochondral and cartilage tissue engineering, Acta Biomater. 57 (2017) 1–25, https://doi.org/10.1016/j.actbio.2017.01.036.

[26] T. Billiet, M. Vandenhaute, J. Schelfhout, S. Van Vlierberghe, P. Dubruel, A review of trends and limitations in hydrogel-rapid prototyping for tissue engineering, Biomaterials 33 (2012) 6020–6041, https://doi.org/10.1016/j.biomaterials.2012.04.050.

[27] D. Loessner, C. Meinert, E. Kaemmerer, L.C. Martine, K. Yue, P.A. Levett, T.J. Klein, F.P.W. Melchel, A. Khademhosseini, D.W. Hutmacher, Functionalization, preparation and use of cell-laden gelatin methacryloyl-based hydrogels as modular tissue culture platforms, Nat. Protoc. 11 (2016) 727–746, https://doi.org/10.1038/nprot.2016.037.

[28] Q. Feng, J.K. Xu, K.Y. Zhang, H. Yao, N.Y. Zheng, L.Z. Zheng, J.L. Wang, K.C. Wei, X.F. Xiao, L. Qin, L.M. Bian, Dynamic and cell-infiltratable hydrogels as injectable carrier of therapeutic cells and drugs for treating challenging bone defects, ACS Cent. Sci. 5 (2019) 440–450, https://doi.org/10.1021/acscentsci.8b00764.

[29] J.M. Townsend, G. Sali, H.B. Homburg, N.T. Cassidy, M.E. Sanders, K.M. Fung, B. T. Andrews, R.J. Nudo, B.N. Bohnstedt, M.S. Detamore, Thiolted bone and tendon tissue particles covalently bound in hydrogel for in vivo calvarial bone regeneration, Acta Biomater. 104 (2020) 66–75, https://doi.org/10.1016/j.actbio.2019.12.035.

[30] Y. Chen, J. Zhang, X. Liu, S. Wang, J. Tao, Y. Huang, W. Wu, Y. Li, K. Zhou, X. Wei, S. Chen, X. Li, X. Xu, L. Cardon, Z. Qian, M. Gou, Noninvasive in vivo 3D bioprinting, Sci. Adv. 6 (2020), eaba7406, https://doi.org/10.1126/sciadv.aba7406.

[31] F.G. Downs, D.J. Lunn, M.J. Booth, J.B. Sauer, W.J. Ramsay, R.G. Klemperer, C. J. Hawker, H. Bayley, Multi-responsive hydrogel structures from patterned droplet networks, Nat. Chem. 12 (2020) 363–371, https://doi.org/10.1038/s41557-20-0444-1.

[32] A. Sun, X. He, L. Li, T. Li, Q. Liu, X. Zhou, X. Ji, W. Li, Z. Qian, An injectable photopolymerized hydrogel with antimicrobial and biocompatible properties for infected skin regeneration, NPG Asia Mater. 12 (2020) 25, https://doi.org/10.1038/s41427-020-0206-y.

[33] Y. Lu, M. Li, L. Li, S. Wei, X. Hu, X. Wang, G. Shan, Y. Zhang, H. Xia, Q. Yin, High-activity chitosan/nanohydroxyapatite/zoledronic acid scaffolds for simultaneous tumor inhibition, bone repair and infection eradication, Mater. Sci. Eng. C 82 (2018) 225–233, https://doi.org/10.1016/j.msec.2017.08.043.

[34] D.J. Li, W. Nie, L. Chen, D. McCoul, D.H. Liu, X. Zhang, Y. Ji, B.Q. Yu, C.L. He, Self-assembled hydroxyapatite-graphene scaffold for photothermal cancer therapy and bone regeneration, J. Biomed. Nanotechnol. 14 (2018) 2003–2017, https://doi.org/10.1166/jbn.2018.2646.

[35] K. Zhang, Y. Zhou, C. Xiao, W. Zhao, H. Wu, J. Tang, Z. Li, S. Yu, X. Li, L. Min, Z. Yu, G. Wang, L. Wang, K. Zhang, X. Yang, X. Zhu, C. Ti, X. Zhang, Application of hydroxyapatite nanoparticles in tumor-associated bone segmental defect, Sci. Adv. 5 (2019), eaax6946, https://doi.org/10.1126/sciadv.aax6946.

[36] R.W.Y. Habash, R. Bansal, D. Krewski, H.T. Alhafid, Thermal therapy, Part 1: an introduction to thermal therapy, Crit. Rev. Biomed. Eng. 34 (2006) 459–489, https://doi.org/10.1615/CritRevBiomedEng.v34.i6.20.

[37] X. Zhang, G. Cheng, X. Xing, J. Liu, Y. Cheng, T. Ye, Q. Wang, X. Xiao, Z. Li, H. Deng, Near-infrared light-triggered porous AuPd alloy nanoparticles to produce mild localized heat to accelerate bone regeneration, J. Phys. Chem. Lett. 10 (2019) 4185–4191, https://doi.org/10.1021/acs.jpclett.9b01735.

[38] L. Tong, Q. Liao, Y. Zhao, H. Huang, A. Gao, W. Zhang, X. Gao, W. Wei, M. Guan, P. K. Chu, H. Wang, Near-infrared light control of bone regeneration with biodegradable photothermal osteoimplant, Biomaterials 193 (2019) 1–11, https://doi.org/10.1016/j.biomaterials.2018.12.008.